Shape-independent permeability model for uniaxially-anisotropic ferromagnetic thin films

Brice Jamieson, Terence O'Donnell, Santosh Kulkarni, and Saibal Roy

Citation: Appl. Phys. Lett. **96**, 202509 (2010); doi: 10.1063/1.3430061
View online: http://dx.doi.org/10.1063/1.3430061
View Table of Contents: http://aip.scitation.org/toc/apl/96/20
Published by the American Institute of Physics

Shape-independent permeability model for uniaxially-anisotropic ferromagnetic thin films

Brice Jamieson, Terence O'Donnell, Santosh Kulkarni, and Saibal Roy[a)]
Microsystems Centre, Tyndall National Institute, University College Cork, Lee Maltings, Cork, Ireland

(Received 28 January 2010; accepted 25 April 2010; published online 19 May 2010)

A permeability model based on the three-dimensional shape demagnetization effect is developed to estimate the permeability of any uniaxially-anisotropic ferromagnetic thin-film for integrated micromagnetic structures. The model is validated by comparison to measured ferromagnetic thin films (NiFe and CoPRe) with different anisotropies and saturation magnetizations. The dependence of permeability on film-thickness is modeled as a function of the demagnetization effect and verified against fabricated samples of varying thicknesses. © *2010 American Institute of Physics*.
[doi:10.1063/1.3430061]

Integrated passive components employing ferromagnetic enhancement layers are of considerable significance in areas such as power conversion,[1] magnetic shielding,[2] radio frequency (rf) applications,[3] magnetic microelectromechanical systems,[4] and magnetic write heads.[5] In all of these applications, the permeability of the ferromagnetic thin films is an important parameter in determining device performance. The permeability of a uniaxially-anisotropic magnetic thin film, however, has been seen to deviate with film shape from that of an as-deposited thin film.[6] This has been observed for measured samples,[7] however, the general-case relationship has yet to be defined. The thickness-dependence of permeability has additionally been shown in the micron-scale for different ferromagnetic materials such as CoTaZr[8] and NiFe.[6] Previous studies, however, have not provided a detailed analysis of the demagnetization effect and instead focused on experimental curve-fitting.[6] This work presents an analytic three-dimensional (3D) model for the initial permeability of an in-plane, uniaxially-anisotropic thin magnetic film, based on the intrinsic material anisotropy and the shape-demagnetization effect described by the rectangular prism model.[9] The model is used to analyze the material-independent effects of film geometry and thickness on permeability and verified for different induced anisotropies and saturation magnetizations by comparison to measured results for CoPRe and NiFe thin films.

Relative permeability in a thin-film, μ_r, is a complex-valued, frequency-dependent function[10] defined in Eq. (1) where δ represents the frequency-dependent skin depth of the film, d represents the film thickness, and μ_{int}, represents the frequency-dependent intrinsic permeability where ferromagnetic resonance has been taken into account. For sufficiently low frequencies Eq. (1) is represented by the initial permeability μ_i, in Eq. (2)[10] where M_s is the saturation magnetization and H_k is the anisotropy field.

$$\mu_r = \mu_{\text{int}}\left[\frac{(1-i)}{d/\delta}\frac{e^{(1+i)d/\delta}-1}{e^{(1+i)d/\delta}+1}\right], \tag{1}$$

$$\mu_i = \frac{Ms}{H_k} + 1 \tag{2}$$

[a)]Author to whom correspondence should be addressed. Electronic mail: saibal.roy@tyndall.ie. Tel.: +353 21 4904331.

The anisotropy, H_k, represents the field required to align all of the magnetic domains in a ferromagnetic material along a given direction. The direction requiring the minimum applied field (and hence energy) to align the magnetic moments is referred to as the easy anisotropy axis. The orthogonal in-plane direction is referred to as the hard anisotropy axis along which a field equivalent to the material anisotropy, H_m, must be applied to align the magnetic moments. The material anisotropy is the sum of induced anisotropy, H_i, magnetocrystalline anisotropy, H_{mc}, magnetoelastic anisotropy, H_{me}, and shape anisotropy, H_d, determined experimentally. H_{mc} and H_{me} arise respectively from the crystal structure, spin-orbit electron interactions, and stress. H_i is the uniaxial anisotropy in the thin-film as an effect of deposition or annealing in a magnetic field, independent of the film shape. Shape anisotropy is a demagnetizing field resulting from dipole interactions at the surface of the film due to the shape of the magnetic body. It acts along an axis in direct opposition to the applied field in that axis and the magnitude varies inversely with the length of the axis. While this is negligible in large samples, it becomes significant as we reduce the film size leading to a micromagnetic structure.

The calculation of shape anisotropy has been determined for various geometries such as the general ellipsoid.[11] Although this is a good approximation of demagnetization, it does not accurately represent the majority of thin-film geometries found in microfabricated devices. A calculation based on a rectangular prism[9] better approximates the very thin, and often rectangular geometries found in uniaxially-anisotropic thin films and thus is adapted in this work to determine the demagnetizing factor, $D(x,y,z)$, along a selected Cartesian axis. Here, x and y are the in-plane axes and the ratio of the lengths along these axes (x/y) is defined as the aspect ratio, AR. The thickness, z, is defined as the out-of-plane axis. The demagnetizing factor along a given axis is inversely proportional to the axis length and must fulfill the requirement that $D_x+D_y+D_z=1$.[11] Thus, any change in the demagnetizing factor of one axis results in a change in the demagnetizing factors in the remaining two axes.

To develop a universal permeability model for a rectangular thin film with dimensions $x \geq y \gg z$, the Stoner–Wohlfarth model[12] is used as a basis. Although this model represents a single-domain particle, it is often an adequate approximation for a discrete system such as a thin film. The

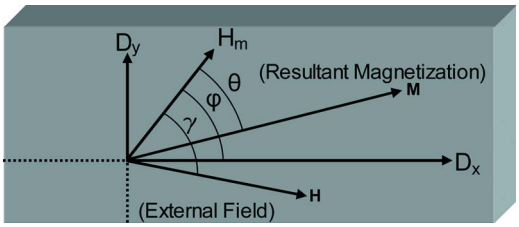

FIG. 1. (Color online) Thin-film representation illustrating incline of material anisotropy axis, θ, from magnetization direction, film rotation axis, φ, and applied field direction, γ with respect to material anisotropy axis.

Stoner–Wohlfarth energy equation for a thin film with shape anisotropy can be given in Eq. (3).[12]

$$E = -K\sin^2\theta - D_x M_s^2\cos^2(\varphi-\theta) - D_y M_s^2\sin^2(\varphi-\theta) + M_s H\cos(\gamma-\theta). \quad (3)$$

In Eq. (3), K represents the hard-axis anisotropy constant. The shape anisotropy is represented by the Cartesian x- and y-components of the 3D shape demagnetizing vector, D, from the rectangular prism model. The x-component of shape anisotropy is aligned at an angle of φ to the anisotropy axis. The Cartesian z-component is considered purely out-of-plane and for such a sample where $x \geq y \gg z$ may be neglected if the magnetizing field is purely in-plane. The applied field energy, $M_s H$, is aligned at an angle of γ with the anisotropy axis. The sample is magnetized along a vector, M, at an angle of θ with the anisotropy axis. This configuration is illustrated in Fig. 1.

For a magnetizing field of H_k, the applied field term can be considered to be equivalent to the anisotropy field, resulting in a magnetic free-energy density of 0. Additionally, the resultant magnetization of the sample aligns with the applied field, causing $M_s H\cos(\gamma-\theta) = M_s H_k$ and $\gamma-\theta=0$. The total energy may be then expressed in Eq. (4) as a rearrangement of Eq. (3), angularly dependent on φ and θ.

$$M_s H_k = K\sin^2\theta + D_x M_s^2\cos^2(\varphi-\theta) + D_y M_s^2\sin^2(\varphi-\theta). \quad (4)$$

The hard-axis anisotropy constant, K, in Eq. (4) assumes that no material anisotropy is present along the easy magnetic axis. A sample with AR=1 is thus typically chosen as the shape anisotropy is expected to be zero. This assumption, however, is incorrect as the shape contribution in Eq. (4) cannot be zero. Anisotropy is thus still observed in both in-plane anisotropy axes, seen for a measured hysteresis curve in Fig. 2. The presence of shape anisotropy is confirmed by Fig. 3, which compares the hard-axis anisotropy in samples

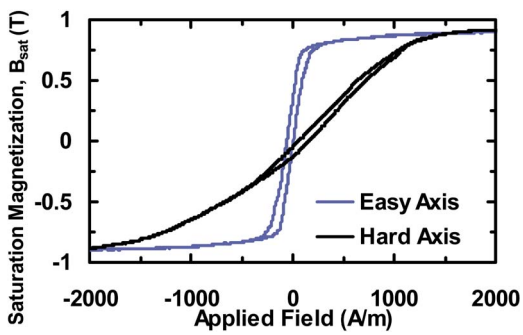

FIG. 2. (Color online) Hysteresis curve for a 10×10 mm^2 sample of 1.5 μm thick $Co_{88.3}P_{11.2}Re_{0.5}$ in the easy and hard anisotropy axes.

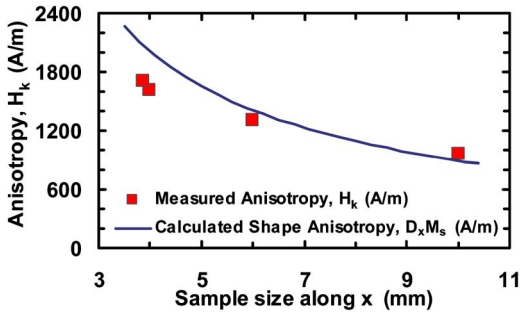

FIG. 3. (Color online) Measured hard-axis anisotropy of a 3 μm thick sample of AR=1 and varied side length vs calculated shape anisotropy.

of various edge sizes and AR=1 to the calculated shape anisotropy for a similar thin film.

To determine the material anisotropy constant, K, the effects of shape anisotropy are extracted from the experimentally measured anisotropy, H_k. This can be done for a sample of AR=1 with the material anisotropy axis along the x axis ($\varphi=0$). The film is measured along the hard anisotropy axis ($\theta=\pi/2$). The difference between the measured easy and hard-axis anisotropies will be equivalent to the material anisotropy and, since $H_m = 2K/M_s$, the equation in Eq. (4) may be rewritten in Eq. (5).

$$\frac{K}{M_s} = \frac{H_m}{2} = H_k - D_y M_s. \quad (5)$$

Using Eq. (5) the material anisotropy may be determined from measurements of a sample with AR=1 and applied to Eq. (4) to calculate the total anisotropy of any rectangular sample made from that material as expressed in Eq. (6), and the initial permeability of such a sample as in Eq. (7).

$$H_k = \frac{H_m}{2}\sin^2\theta + M_s[D_x\cos^2(\varphi-\theta) + D_y\sin^2(\varphi-\theta)], \quad (6)$$

$$\mu_i = \frac{M_s}{\frac{H_m}{2}\sin^2\theta + M_s[D_x\cos^2(\varphi-\theta) + D_y\sin^2(\varphi-\theta)]}. \quad (7)$$

To confirm the thin film, uniaxial permeability model, thin films were prepared with various aspect ratios and the anisotropy and permeability measured and compared to calculated values. A sample of 1.5 μm thick $Co_{88.3}P_{11.2}Re_{0.5}$ with in-plane anisotropy was electrodeposited on a 4″ Si wafer in the presence of a 13.6 kA/m magnetic field.[13] The

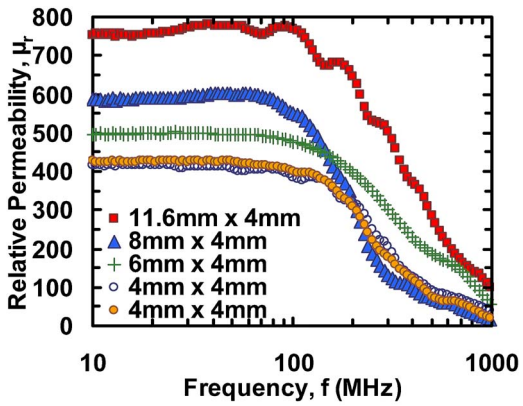

FIG. 4. (Color online) Real part of complex permeability for a 1.5 μm thick $Co_{88.3}P_{11.2}Re_{0.5}$ sample of varying aspect ratio.

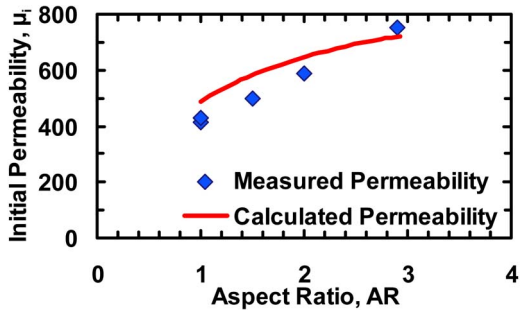

FIG. 5. (Color online) Measured and calculated initial permeability vs aspect ratio for a 1.5 μm thick, 4 mm wide $Co_{88.3}P_{11.2}Re_{0.5}$ sample showing the easy material axis aligned along x.

material anisotropy, H_k', was determined experimentally with a hysteresis loop tracer (SHB Electronics—model: MESA) to be 1056 A/m in a sample cut from this wafer with AR =1 and 10 mm to a side. Using Eq. (5), H_m was calculated to be 1460 A/m. Samples were diced from this wafer with the hard anisotropy axis along the x (hard) direction, which was varied from 4 to 11.6 mm, and y (easy) and z directions held constant at 4 mm and 1.5 μm, respectively. The permeability for the samples in Fig. 4 was measured in the x direction from 1 MHz to 9 GHz with a permeameter (Ryowa Electronics—model: PMM-9G1). The initial permeability was taken from the 1 MHz point of the frequency spectrum and compared to the modeled permeability in Fig. 5, showing a good agreement between the modeled and measured permeabilities. Figure 6 illustrates the angular-dependence of anisotropy for an 11.6×4 mm^2 $Co_{88.3}P_{11.2}Re_{0.5}$ sample as γ is rotated from $\pi/2$ to $3\pi/2$. The material anisotropy angle, θ, is $\pi/2$, representing the material hard anisotropy axis aligned along the long sample direction. The measured values in Fig. 6 match well with the calculated material anisotropy. This, along with the accurate prediction of initial permeability, validates this model for measurements independently of the shape and orientation of the sample.

This model may additionally be used to predict the thickness-dependence of permeability. In this case the thickness, z, is varied with a fixed ratio of x to y. An increasing value of z will reduce D_z and subsequently increase D_x and D_y, reducing the in-plane initial permeability as in Eq. (7). To confirm this, a set of electrodeposited $Ni_{45}Fe_{55}$ samples[6]

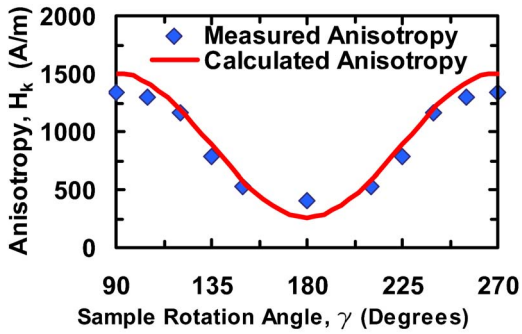

FIG. 6. (Color online) Measured anisotropy for a 1.5 μm thick, 11.6 $\times4$ mm^2 $Co_{88.3}P_{11.2}Re_{0.5}$ sample rotated through 2π from the long sample direction and compared to calculated anisotropy.

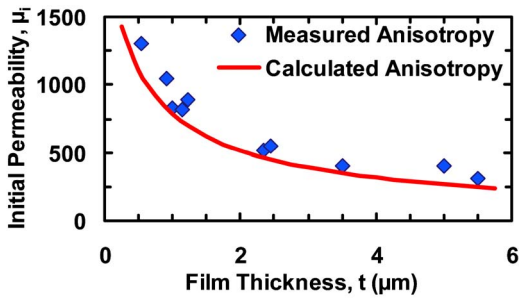

FIG. 7. (Color online) Thickness dependence of permeability for a 3.5 $\times3$ mm^2 $Ni_{45}Fe_{55}$ sample compared to calculated values.

of varying thicknesses and constant AR was analyzed with the easy magnetic axis along x. The saturation magnetization of these samples is 1.15×10^6 A/m and the material anisotropy is 1073 A/m as measured from hysteresis curves and corrected for shape using Eq. (5). Figure 7 shows the calculated permeability of the samples compared to the measured values if thickness is varied between 500 nm and 2.5 μm. The figure shows a good fit of the developed model to the measured data and matches closely with the thickness-dependence relation presented by O'Donnell *et al.*,[6] $\mu_i = 900\ z^{-0.5}$. This confirms the capacity of this model to predict the thickness-dependence of permeability. The material-independence of this model is confirmed by the fit to various materials as described earlier in Figs. 5–7.

In conclusion, 3D analytic models for shape anisotropy were used to develop a model for the permeability of a rectangular thin film. The shape-dependency and thickness-dependency of the demagnetizing factor and its effect on permeability are calculated using this model and shown to be in good correlation with values obtained experimentally. Using this model, the permeability of a magnetic core may be calculated for any size of thin film, allowing for more accurate predictions requiring only the measurement of saturation magnetization and anisotropy.

This work was supported by EI CFTD/2008/331 and SFI 06/IN.1/I98. The authors would like to thank Dr. Ningning Wang, Paul McCloskey, and Dr. Jan Kubik.

[1]S. Prabhakaran, T. O'Donnell, C. R. Sullivan, M. Brunet, S. Roy, and S. C. O'Mathuna, J. Magn. Magn. Mater. **290–291**, 1343 (2005).
[2]Y. P. Su, X. Liu, and S. Y. Hui, IEEE Trans. Power Electron. **23**, 2052 (2008).
[3]V. Korenivski and R. B. van Dover, J. Appl. Phys. **82**, 5247 (1997).
[4]E. Flick, K. Feindt, and H. H. Gatzen, IEEE Trans. Magn. **44**, 3973 (2008).
[5]M. Yoshino, Y. Kikuchi, A. Suiyama, and T. Osaka, Electrochim. Acta **53**, 285 (2007).
[6]T. O'Donnell, N. Wang, S. Kulkarni, R. Meere, F. M. F. Rhen, S. Roy, and S. C. O'Mathuna, J. Magn. Magn. Mater. **322**, 1690 (2010).
[7]D. W. Lee and S. X. Wang, J. Appl. Phys. **103**, 07E907 (2008).
[8]D. S. Gardner, G. Schrom, P. Hazucha, F. Paillet, T. Karnik, S. Borkar, R. Hallstein, T. Dambrauskas, C. Hill, C. Linde, W. Worwag, R. Baresel, and S. Mutuhumar, J. Appl. Phys. **103**, 07E927 (2008).
[9]A. Aharoni, J. Appl. Phys. **83**, 3432 (1998).
[10]E. van de Riet and F. Roozeboom, J. Appl. Phys. **81**, 350 (1997).
[11]J. A. Osborn, Phys. Rev. **67**, 351 (1945).
[12]E. C. Stoner and E. P. Wohlfarth, Philos. Trans. R. Soc. London A **240**, 599 (1948).
[13]D. S. Gardner, P. McCloskey, B. Jamieson, S. Roy, and T. O'Donnell, U.S. Patent No. 20090169874 A1 (pending).